Influence of Nucleation on the Brittle-Ductile Transition Temperature of Impact-Resistant Polypropylene Copolymer: From the Sight of Phase Morphology

Dong Cheng,[1] Jiachun Feng,[1] Jianjun Yi[2]

[1]*Key Laboratory of Molecular Engineering of Polymers of Ministry of Education, Department of Macromolecular Science and Laboratory of Advanced Materials, Fudan University, Shanghai 200433, People's Republic of China*
[2]*Key Laboratory of Synthetic Resin, Institute of Petrochemical Technology, China National Petroleum Corporation, Beijing 100083, People's Republic of China*

Received 29 December 2010; accepted 7 April 2011
DOI 10.1002/app.34639
Published online 19 August 2011 in Wiley Online Library (wileyonlinelibrary.com).

ABSTRACT: Influence of α- and β-nucleation on brittle-ductile transition temperature (BDTT) of impact-resistant polypropylene copolymers (IPCs) and their phase morphologies were comparatively investigated. Impact test showed that the BDTT of β-nucleated IPC (β-IPC) is ~ 24°C lower than that of α-nucleated one (α-IPC). Structural characterizations including atomic force and scanning electron microscopic observations, small angle X-ray scattering examination, and dynamical mechanical analysis revealed that dispersion of the ethylene-propylene random copolymer-rich (EPR-rich) phase was finer in β-IPC in comparison with that in α-IPC. For the reason of looser lamellar arrangement, the portion of EPR-rich components included in the interlamellar region of β-IPC was higher than those of α-IPC, which led to improved mobility for the amorphous polypropylene chains. It was proposed that the finer distribution of EPR-rich phase, which might result from faster growth rate of the β-crystal and looser lamellar arrangement of β-spherulite, should be responsible for the improved impact-resistance and lower BDTT in β-IPC samples. © 2011 Wiley Periodicals, Inc. J Appl Polym Sci 123: 1784–1792, 2012

Key words: impact-resistant polypropylene copolymer; brittle-ductile transition temperature; crystallization; phase morphology

INTRODUCTION

Isotactic polypropylene (iPP) is one of the most widely used materials, owing to its light weight, chemical and electrical resistance, relatively low cost, and excellent processability properties. However, the poor impact resistance of iPP and its sensitivity to notch,[1,2] particularly at low temperature disenable it to be used as an engineering plastic. Incorporating a discrete rubbery phase is believed to be an effective way to toughen iPP. In this field, no great progress was achieved until the invention of porous spherical $TiCl_4/MgCl_2$ catalyst and so-called "reactor granule technology" (RGT).[3,4] Productions made by RGT are commonly called impact-resistant PP copolymer (IPC), high-impact PP, or polypropylene (PP) in-reactor alloys. Early studies on IPC showed that it has complex composition and phase structure.[5–7] That is, in addition to the main components of crystalline iPP and amorphous ethylene-propylene random copolymer (EPR), there also exist some partially crystalline ethylene-propylene block copolymers (EPBs) with varying segmental lengths, and all of these components combine into a complex core-shell multilayer structure. So far, the most concerned topic in the research of IPC is clarifying the origination of its excellent rigidity-toughness balance property. By understanding this structure–property relationship, it will in return enable rational design of IPC materials and optimize their properties through improvements in polymerization and process technology. Although it is generally believed that the excellent rigidity-toughness balance of IPC is associated with its complex composition and phase structure, a complete understanding on the relationship of its final performance with structure at different scales has not been achieved yet.

In a simple approximation, components in IPC can be divided into two categories, the crystalline ones (i.e., iPP, and partially crystalline polymers with long PE or PP segments, denoted as PP-rich components) and the amorphous ones (i.e., EPR and iPP with very low isotacticity, denoted as EPR-rich components). The mechanical properties, including rigidity and

Correspondence to: J. Feng (jcfeng@fudan.edu.cn).
Contract grant sponsor: Natural Science Foundation of China; contract grant number: 20874017.
Contract grant sponsor: Shanghai-Unilever Research & Development Fund; contract grant number: 09520715500.
Contract grant sponsor: National Basic Research Program of China; contract grant number: 2011CB605700.

toughness, of IPC are largely determined by phase structure as well as their mutual interactions. In blend that consists of both crystallizable and amorphous parts, crystallization, and liquid–liquid phase separation (LLPS) are two common transitions, which determine the phase morphology of the sample. Hence, a deeper understanding of the interplay between crystallization and phase separation in polymer blends holds enormous technological and scientific importance. In such blends, the noncrystalline phase can be rejected into interlamellar, interfibrillar, or interspherulitic region during the crystallization.[8] It was proposed by Keith and Padden[9,10] that the scale of segregation was quantitatively depended on a parameter, which was expressed by $\delta = D/G$, where δ is the dimensional order of segregation, D is the diffusion coefficient of the noncrystalline component, and G is the spherulitic radial growth rate. This was confirmed by Inaba et al.[11,12] who found that in PP/EPR blend, the modulated structure developed by phase separation was conserved if the rate of crystallization was much faster than that of mutual diffusion of the constituent polymer molecules but was not conserved if the crystallization rate was sufficiently slow compared with the rate of mutual diffusion. Crystallization may induce abnormal phase separation process. Phase contrast microscopy observation for the mixture of poly (ε-caprolactone)/polystyrene carried out by Tanaka et al.[13,14] showed a local phase separation at the growth front of the spherulites during the crystallization, which was mainly caused by the preferential rejection of impurities during crystallization. On the contrary, the LLPS also has effect on the crystallization. Recently, Han et al.[15–17] found that enhanced concentration fluctuations at the diffuse interface of the immiscible polymers could greatly facilitate the nucleation process for crystallization.

As is known, α- and β-forms are two main modifications of iPP. The monoclinic α-modification is thermodynamically stable and has good mechanical strength. It owns a unique cross-hatching crystalline texture, which is consisting of radial- and high-angle- (80 or 100°) branched tangential lamellae,[18] which is generally attributed to the small mismatch between the *a*- and *c*-axes in the two sets with the (010) planes in conduct.[19,20] The PP in dominantly trigonal β-modification usually shows enhanced toughness in comparison with that in α-modification. It is generally accepted that improved toughness is attributed to the energy dissipation during yield process accompanied by phase transformation from β- to α-forms and the loose structure of β-form crystals (compared with α-crystals) in favor of a absorbing impact energy.[21,22] Fu et al.[23] proposed that the particular connection mode between crystallites might be also the main reason for the improved toughness of β-iPP. In previous works, it has been proved that the growth rate of β-spherulite is higher than that of α-spherulite in a critical temperature range (around 105 ~ 140°C).[24–26] Considering their differences in crystallization rate and crystal structure, which will inevitably change the phase separation process and subsequently the final mechanical properties, it is reasonable to speculate that phase morphology as well as the resultant mechanical properties for β-nucleated IPC (β-IPC) may be different from that for its α-nucleated counterpart (α-IPC). Recently, Bai et al.[27,28] and Grein et al.[29,30] found that the introduction of β-nucleating agent would greatly improve the toughness of PP/rubber blends, and even resulted in a shift of brittle-ductile transition temperature (BDTT) to a lower temperature in some blends. BDTT is an important criterion in materials selection since, once a material is cooled below this temperature, it has much greater tendency to shatter on impact instead of bending or deforming. Lowering value of BDTT without further increasing the rubbery content, which means improving the toughness at low temperature while keeping its rigidity at relative higher temperature, is especially meaningful for IPC. This could endow IPC with superior rigidity-toughness balance and extend its lowest service temperature. To the best of our knowledge, no similar work has been reported on IPC, and the mechanism for lowering of BDTT in thus system is far away from a clear understanding.

In this work, IPC samples in dominantly α- and β-modifications were, respectively, prepared by introducing small amount of α- or β-nucleating agents, and their differences in impact-resistant behaviors, especially the BDTT, were comparatively investigated. It was found that the BDTT is significantly lower for β-IPC than that for α-IPC, which indicated that the existence of EPR-rich amorphous phase and β-modification showed a synergistic improvement on the toughness of iPP. Morphological characterizations showed that dispersion of EPR-rich phase in β-IPC was much finer. On the basis of our observation and characterizations, possible explanations for these differences were proposed.

EXPERIMENTAL

Materials and sample preparation

IPC (SP179) with $M_w = 1.53 \times 10^5$ g/mol, $M_w/M_n \sim 5.02$, ethylene content of about 10.6%, and MFR = 9.7 g/(10 min) is a commercial product produced by Qilu Petrochemical Co., SINOPEC (Shandong, China). The α-nucleating agent (α-NA) used is 1, 3 : 2, 4-bis(3,4-dimethylbenzylidene) sorbitol (DMDBS; Millad), and β-nucleating agent (β-NA) is a two-component mixture of pimelic acid and calcium stearate (weight ratio 1 : 1).

α- and β-NA (0.1 wt %) were melt blended into the IPC using an SHJ-38 corotating twin screw extruder (Lanzhou, China) with a L/D ratio of 30, respectively. A temperatures profile of 170–230°C from hopper to die was applied. After granulation, standard specimens ($80 \times 10 \times 4$ mm^3) for impact test were injection-molded by an HTF86X1 injection-molding machine (Changchun, China) with temperatures of 190–210°C from hopper to nozzle and mold temperature of 30°C. To investigate the multistructure of the two samples, the preblended granulates were molded into 0.5-mm-thick sheets at 200°C under a pressure of 15 MPa for 5 min and then cooled naturally to room temperature before being tested.

Mechanical test

After the specimens were conditioned at the selected temperature (varied in between −30 and 40°C at temperature intervals of 10 or 5°C) for at least 4 h, impact resistance was tested immediately using an XJJ impact tester (Zhineng, China) according to GBT-1043-93. The impact strength was derived from average value of at least seven specimens.

Before dynamic mechanical analysis (DMA) test, the 0.5-mm-thick sheets were cut into rectangular cross-sectional bars with size of $30 \times 5 \times 0.5$ mm^3, and then they were tested using a NETZSCH 242C dynamic mechanical analyzer (Netsch, German). Single cantilever mode was selected, and the measurement was carried out from −80 to 120°C, at the heating rate of 3°C/min and frequency of 1 Hz.

Differential scanning calorimetry

Thermal behaviors of both samples were measured on a Mettler DSC-1 apparatus (Mettler Toledo, Switzerland) in a nitrogen atmosphere. The differential scanning calorimetry (DSC) traces of first heating scan from 30 to 200°C for samples cut from those 0.5-mm-thick sheets were recorded at the heating rate of 10°C/min, and the degree of crystallinity (X_c) was calculated by:

$$X_c(\%) = \frac{\Delta H_{\mathrm{m,iPP}}}{\Delta H^0_{\mathrm{m,iPP}} \times \omega_{\mathrm{iPP}}} \times 100\% \quad (1)$$

where $\Delta H_{\mathrm{m,iPP}}$ is the measured apparent melting enthalpy of iPP, $\Delta H^0_{\mathrm{m,iPP}}$ is the enthalpy corresponding to the melting of a 100% crystalline sample, and ω_{iPP} is the weight fraction of iPP in IPC (about 77 wt %). Here, the values of $\Delta H^0_{\mathrm{m,iPP}}$ for α- and β-PP are selected as 177.0 and 168.5 J/g, respectively.[31]

Wide angle X-ray diffraction

Wide angle X-ray diffraction (WAXD) measurements were performed on the 0.5-mm-thick sheets using a PANalytical X'pert diffractometer (PANalytical, Netherlands) in the reflection mode with Ni-filtered CuKα radiation ($\lambda = 0.154$ nm) under 40 kV and 40 mA. Radial scans of intensity versus diffraction angle 2θ were recorded in the region of 5–25°. The β-phase fraction (K_β) was calculated following the equation[32]:

$$K_\beta = \frac{H^\beta_{300}}{H^\alpha_{110} + H^\alpha_{040} + H^\alpha_{130} + H^\beta_{300}} \quad (2)$$

where H^α_{110}, H^α_{040}, and H^α_{130} are the intensities of the (110), (040), and (130) reflections of the α-phase, respectively, and H^β_{300} is the intensity of (300) reflection of β-phase.

Scanning electron microscopy

The 0.5-mm-thick sheets were first cryogenically fractured in the direction perpendicular to flow direction, then the newly fractured surfaces were etched in a mixed solution of 1.3 wt % potassium permangate ($KMnO_4$), 32.9 wt % hydrochloric acid, and 65.8 wt % concentrated sulfuric acid for about 4 h, according to the procedure proposed by Olley et al.[33] The phase morphology and supermolecular structure of the samples were observed using a TS 5136MM scanning electron microscopy (SEM; TESCAN, Germany) with an accelerating voltage of 20 kV.

Atomic force microscopy

Small amount of α- and β-IPCs were, respectively, melted and pressed into films around 50 μm in thickness between two clean silicon wafers. Tapping mode atomic force microscopy (AFM) was performed on these films using a NanoScope IV Multi-Mode AFM (Veeco Instruments), whereby both height and phase images were obtained. Before analyzing, the images were properly flattened using AFM software to eliminate the height errors.

Small angle X-ray scattering

Small angle X-ray scattering (SAXS) measurement was performed on the 0.5-mm-thick IPC sheets with a NanoStar U SAXS System (Bruker, Germany). The X-ray beam used was CuK_α radiation, and the scattering data were collected using a Bruker Hi-Star two-dimensional real time probe in the small 2θ range of 0.2–2.8°. The scattering intensity $I(q)$ was transformed to $I(q)q^2$ for the correction of Lorentz factor, where q is a scattering vector defined as $q = (4\pi/\lambda)\sin\theta$. The long period ($L$) was calculated from the maximum of the diffuse intensity by $L = \frac{2\pi}{q_{\max}}$, where $q_{\max}$ corresponds to the maximum of the scattering curve.

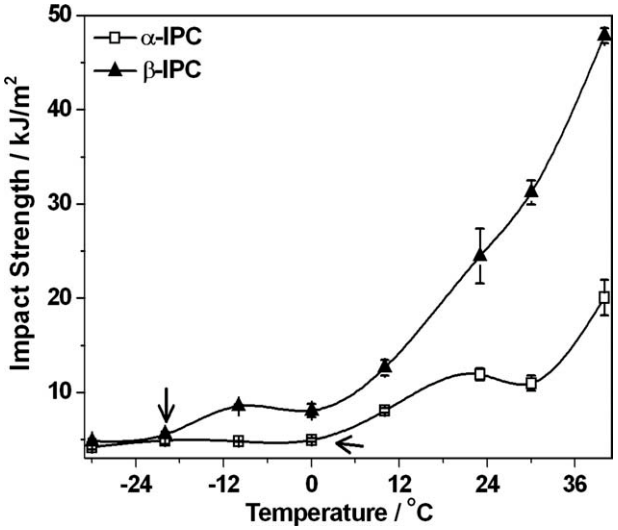

Figure 1 Plot of Charpy impact strength versus temperature; the arrows denote the temperatures at which the brittle-ductile transitions occur.

RESULTS AND DISCUSSIONS

Determination of the mechanical properties

Figure 1 shows the dependence of notched Charpy impact strength on conditioning temperature (T_{cd}) for α- and β-IPCs. It can be seen that within the temperature range adopted in the work, the impact strength follows a similar trend for both samples. At relative low T_{cd}, the impact strength is low and appears to be independent of the temperature. With the increase of T_{cd}, the impact resistance raises upward a plateau with higher value and then sharply increases with the further raise in T_{cd}. However, the differences between these two samples are also displayed. First, at a large temperature range, that is, higher than −20°C, the impact resistance of β-nucleated sample is higher than that of its α-nucleated counterpart, and the increment becomes more prominent with the increase of test temperature. For example, the impact strength of β-IPC at 23°C (24.4 kJ/m^2) is around two times of that for α-IPC (11.8 kJ/m^2). It reveals that the toughness of β-nucleated sample is much improved in comparison with α-nucleated one, which is consistent with the results of early reports.[26–30] Second, at temperature range of 0 ~ 20°C for α-IPC and −25 to −10°C for β-IPC, respectively, the value of impact strength increases with T_{cd} from lower plateau to the higher one, which is just corresponding to the fracture manner of these samples transiting from brittle to ductile (BDT). Herein, BDTT is assigned to be the beginning temperature of obvious increase in impact strength (denoted by the arrow in Fig. 1), which is about 4°C for α-IPC and −20°C for β-IPC, respectively. It is notable that BDTT lowered about 24°C for β-IPC in comparison with the α-nucleated sample, which is desirable for expanding the service temperature of IPC. Considering that the chemical components of α- and β-IPCs used in this work are almost same, and the proportion of EPR-rich components does not change with the introduction of nucleating agents, it is reasonable to propose that the remarkable differences in toughness as well as BDTT may be closely related to the variations in phase morphology and supermolecular structures. To study the probable mechanism for the different impact behaviors, a comparative investigation on multistructures of these samples is needed.

Crystalline modification

The DSC traces of first heating scan and WAXD profiles for α- and β-IPC samples cut from the 0.5-mm-thick sheets were recorded and shown in Figure 2. On the DSC endotherms, the melting peaks located at around 165 and 152°C belong to the α- and β-modifications, respectively, and the lower melting peak at around 115°C is attributed to the melting of crystalline segments in EPB.[5] It clearly shows that

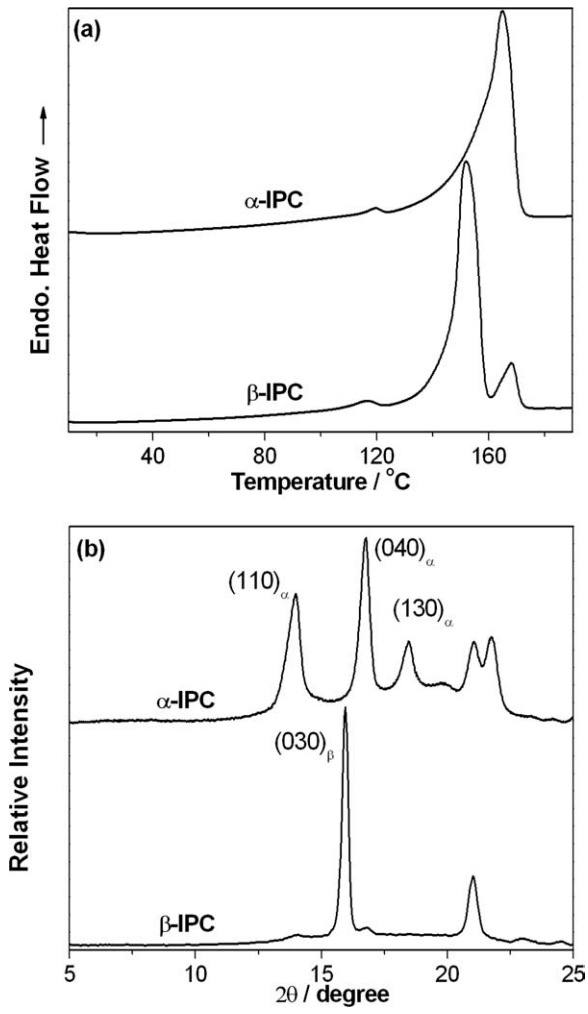

Figure 2 DSC melting traces (a) and WAXD profiles (b) for the α- and β-IPCs.

TABLE I
Parameters Obtained from the DSC and WAXD Examinations

Samples	$T_{m\alpha}$[a] (°C)	$T_{m\beta}$[a] (°C)	X_c (%)[b]	K_β (%)[b]
α-IPC	164.9	–	49.7	–
β-IPC	168.2	151.8	48.4	89.2

[a] Determined by DSC.
[b] Determined by WAXD.

dominantly α- and β-phases present in α- and β-IPCs, respectively. This is further confirmed by WAXD results [Fig. 2(b)]. On the WAXD patterns of α-IPC, there are five local maxima at the 2θ values of ~ 14.0, 16.8, 18.6, 21.2, and 21.8°, corresponding to the (110), (040), (130), and overlapping (131) and (111) reflections, which are characteristic peaks of monoclinic α-form. On the contrary, almost no features associated with α-modification but two peaks that stand for the β-crystalline phase at 2θ values of 16.0° representing the (300) plane and of 21.0° accounting the (301) plane are observed on the WAXD patterns of β-IPC. The detailed data including the crystallinity (X_c) calculated using Eq. (1) and the relative content of the β-modification (K_β) calculated using Eq. (2) for both samples are listed in Table I. In brief, the outcomes of DSC and WAXD confirm that the dominantly crystalline modifications are α- and β-forms in α- and β-IPCs, respectively. Thus, they are ideal samples for the comparative studies on the effects of nucleation on the phase morphologies of IPCs.

Supermolecular structures

Figure 3 shows SEM images of α- and β-IPC samples, respectively. After proper etching procedure, the rubbery phase is partially removed, which corresponds to the holes in the SEM micrographs. In images with smaller magnification [Fig. 4(a,b)], two types of cavities can be seen: big ones (5 ~ 10 μm in diameter) with irregular shapes and small ones (0.1 ~ 1 μm in diameter) with spherical shape, which should correspond to two types of segregation scale

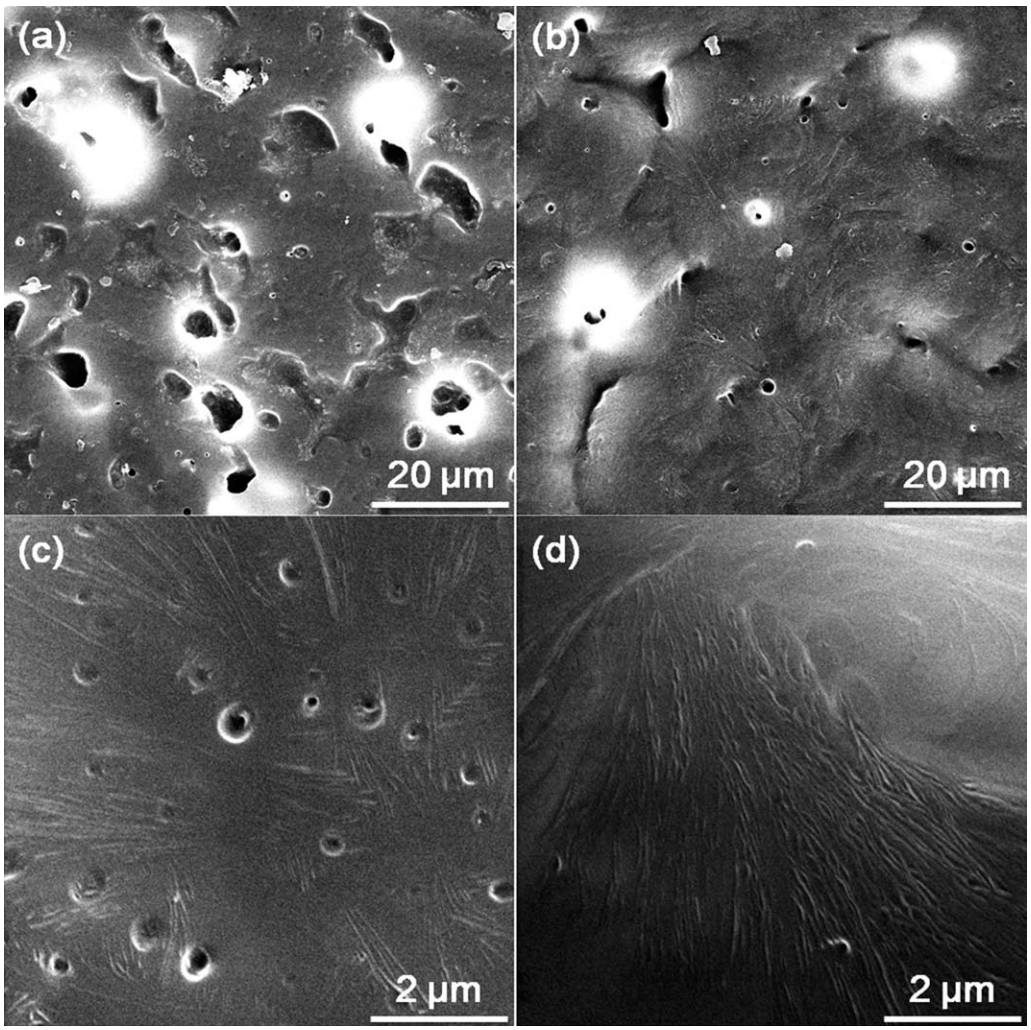

Figure 3 SEM micrographs for α-IPC (a, c) and β-IPC (b, d) at the magnifications of 2,000 (a, b) and 20,000 (c, d).

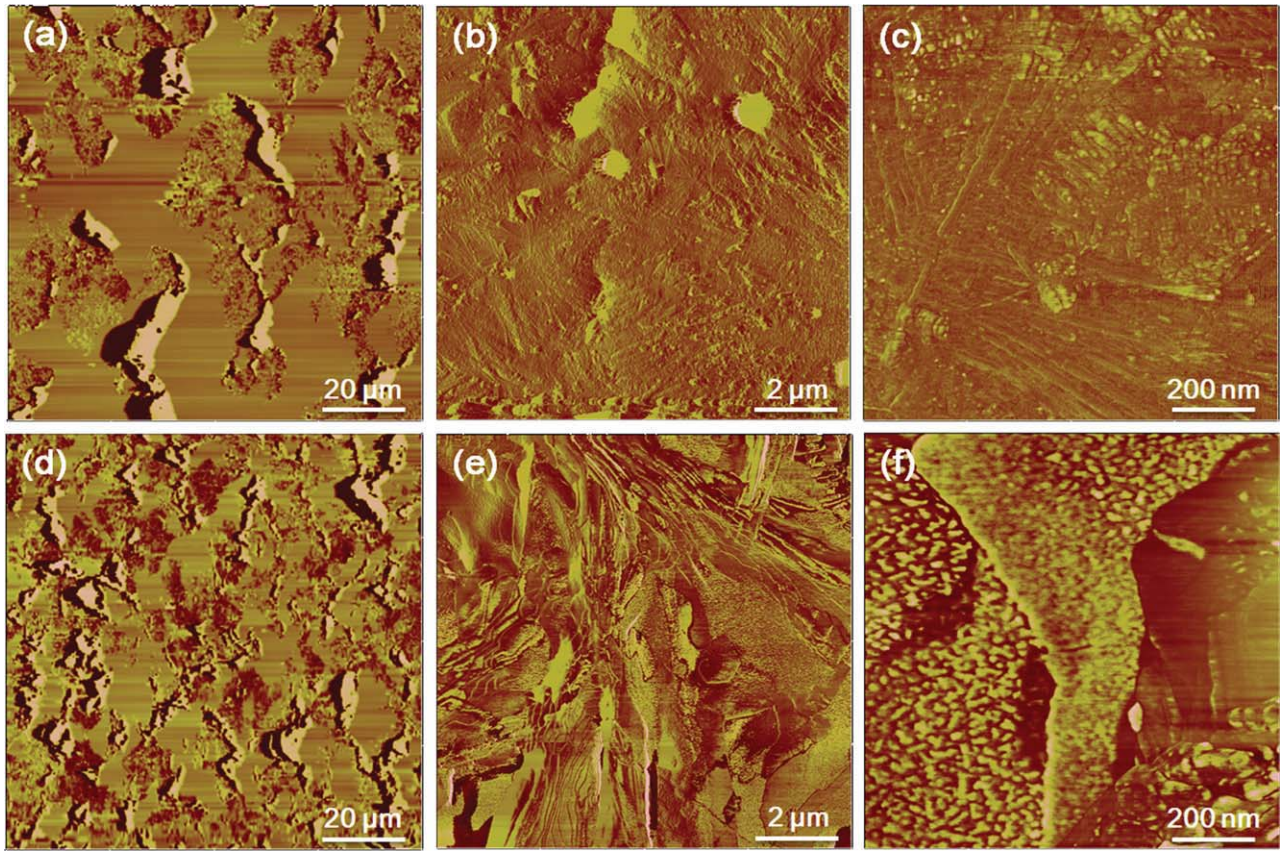

Figure 4 AFM phase images of α-IPC (a–c) and β-IPC (d–f) with the scanning size of 100 × 100 μm^2 (a and d), 10 × 10 μm^2 (b and e), and 1 × 1 μm^2 (c and f). [Color figure can be viewed in the online issue, which is available at wileyonlinelibrary.com.]

for EPR-rich components: bigger ones are the consequence of EPR-rich components separated into interspherulitic region, while the smaller ones correspond to those being rejected into interfibrillar region.[13,14] It is clearly seen that the cavities in the image of α-IPC were more and larger than those in image of β-IPC, which indicates EPR-rich components in the former sample are largely aggregated. That is to say, the dispersion of EPR-rich phase is finer in β-IPC than in the α-nucleated counterpart. Micrographs of larger magnification further show the morphologies of crystalline phase for both samples, and the EPR-rich phases in the crystalline phase can be seen more clearly, as is displayed in Figure 3(c,d). The image of α-IPC shows the typical cross-hatched lamellae arrangement while that of β-IPC displays the flat-on and edged-on lamellae structures. Unlike the globular cavities in α-IPC, the cavities in β-nucleated sample are smaller in size and seem to be elongated in shape, which are more likely the gaps between lamellae. The SEM observation suggests that more proportion of EPR-rich components in β-IPC may be rejected into interlamellar region of the crystal in comparison with in α-IPC. That is to say, the segregation distance for more portion of EPR-rich phase in β-IPC is shorter, and therefore, the amorphous components are less aggregated.

AFM has also been used to distinguish the rubbery and the crystalline components in IPC. Figure 4(a) and (d), respectively, show the phase images of α- and β-IPCs at low magnification. The minor phase with brighter color corresponds to the EPR-rich rubbery phase, while the rest corresponds to the crystalline phase. The nonspherical shape of the rubbery phase may be originated from rejection of the random distributed crystal spherulites during crystallization. It is clear that the EPR-rich phase's domain size is much smaller in β-IPC in comparison with that in α-IPC. The phase image of larger magnification for α-IPC [Fig. 4(b)] shows a flat morphology of compact α-lamellar arrangement and small amount of spherical rubbery components distributed in it. Comparatively, enlarged phase image for crystalline phase of β-IPC [Fig. 4(e)] shows relative loose crystalline phase morphology for the reason of appearing of edged-on and flat-on lamellae. Instead of the spherical shape of rubbery components, larger interlamellar gaps are emerged in the crystalline phase of β-IPC. On the further enlarged phase images for crystalline phase of both samples, the cross-hatched

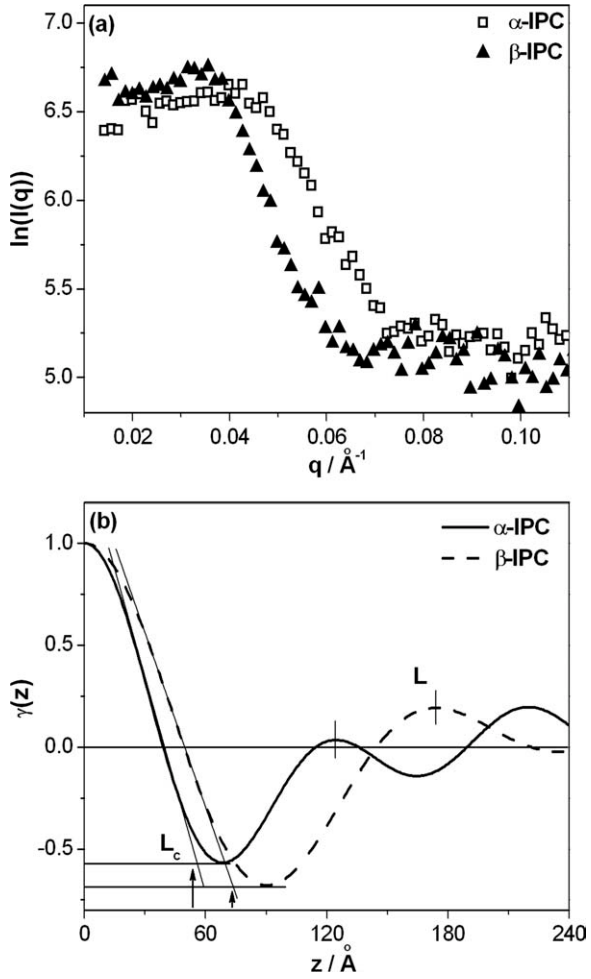

Figure 5 SAXS patterns (a) and one-dimensional correlated SAXS curve (b) for two IPC samples (L: long period and L_c: lamellae thickness).

morphology of the lamellae in α-IPC sample [Fig. 4(c)] as well as the flat-on and edged-on lamellae in β-IPC [Fig. 4(f)] can be observed clearly. These results are in good agreement with what obtained from SEM observation.

Possible mechanism

SAXS is carried out to further study the probable mechanism for the finer dispersion of EPR-rich phase in β-IPC. As shown in Figure 5, SAXS profiles for both IPC samples show one maximum scattering intensity, and it positions at lower q value for β-IPC compared with its α-nucleated counterpart. One-dimensional correlation function technique is applied to get information about the long period (L), lamellar thickness (L_c), and interlamellar distance (L_a). The correlation function expresses as follows[34]:

$$\gamma(z) = \frac{\int_0^\infty I(q)q^2 \cos(qz)dq}{\int_0^\infty I(q)q^2 dq} \quad (3)$$

where z is the correlation distance along the direction from which the electron density distribution is measured. The structure parameters determined from correlation results are given in Table II. These results suggest that not only the long period but also the interlamellar distances are much larger for β-IPC in comparison with those for α-nucleated sample.

As is known, the final phase morphology is determined by the LLPS, which can be affected by many factors. There is no doubt that our morphological characterizations on α- and β-IPC samples have verified a much improved distribution of EPR-rich phase in the latter one. We speculate that this is closely related to the competition between LLPS and crystallization. It is worth mentioning that the IPC blend owns a UCST-type phase diagram, as has been proved by Li et al.[35] To illustrate the effect of nucleation on the phase morphology of IPC, the Keith-Padden parameter (δ) that is positively relative to the segregation distance of the noncrystalline impurities from the growth front, can be used. It is well known that the growth rate of β-spherulite is faster than that of α-spherulite in a critical temperature range (about 105 ~ 140°C),[24–26] which partially overlaps with the dominant temperature range that crystallization happens along with the cooling of both IPC samples. The faster growth rate will result in a smaller δ value for β-IPC than that of α-IPC. In other words, the segregation distance of the EPR-rich amorphous phase induced by crystallization in β-IPC is shorter, which corresponds to less aggregated EPR-rich phase. This may contribute to one possible explanation for why better dispersion of EPR-rich phase is achieved in β-IPC compared with that in α-IPC.

The difference in compactness of the crystalline phase may be the other reason for the differences in final phase morphology. As has been verified by AFM, SEM, and SAXS, looser lamellar arrangement (longer interlamellar distance) is present in β-IPC in comparison with that in α-one. Hence, more portions of EPR-rich components in β-IPC would be rejected into these regions during the crystallization process, which lead to less aggregated rubbery phase in interspherulitic regions. It has been confirmed by Tanaka et al.[14] and Khambatta et al.[36] that the interlamellar spacing increased with the increased

TABLE II
Structure Parameters Obtained from SAXS Correlations

Sample	Long period (L)/nm	Lamellar thickness (L_c)/nm	Interlamellar distance (L_a[a])/nm
α-IPC	12.4	5.5	6.9
β-IPC	17.4	7.3	10.1

[a] $L_a = L - L_c$.

inclusion of noncrystalline rubber in the interlamellar region. For the reason of complex composition of IPC sample, it is hard for us to carry out such a specific comparison. Nevertheless, if the inclusion of the EPR chains in interlamellar regions becomes increased, the mobility of the amorphous PP chains in these regions will be improved correspondingly, which may be confirmed by DMA.

DMA profiles of loss factor for α- and β-IPCs are shown in Figure 6. The peaks positioned around −30 (T_{EPR}), 20 (T_{iPP}), and 80°C ($T_{\alpha c}$) may be attributed to glass transition temperature (T_g) of EPR, β-relaxation of amorphous PP in the crystalline phase, and diffusion of crystallographic defects, respectively.[37] As is indicated by the inset of Figure 6, the peak T_{EPR}, which may be associated with the dispersion of the EPR-rich phase, is boarder for β-IPC in comparison with that for α-IPC. For β-nucleated iPP homopolymers, Labour et al.[37] found that the peak T_{iPP} shifted to higher temperature for the reason of numerous tie molecules in β-nucleated samples. However, in the present work, we find that the peak shifts to lower temperature in β-IPC sample in comparison with that in α-nucleated one. This indicates that the mobility of the amorphous PP chains in β-IPC is improved, which may originate from the inclusion of more EPR chains in the crystalline phase. The DMA results support our speculation that more content of EPR chains may be included in the interlamellar region of PP. It has been reported.[38,39] that there is a positive correlation between the impact strength and the relaxation peak area of matrix's β-relaxation (I_R) in DMA curves, and the larger the area of the loss peak, the higher the value of impact strength. The I_R values calculated from peak T_{iPP} on DMA curves are listed in Table III. As is seen, the I_R value of β-IPC (0.643) is nearly two times of that for α-IPC (0.345), revealing that the impact strength for β-IPC is much higher than that for α-IPC, which is in good agreement with the results obtained from Charpy impact resistance test. For the peak $T_{\alpha c}$, it is lower for β-IPC than that for α-nucleated sample, which suggests an easier activation of the crystal defect in β-IPC. This contributes to the increment in impact strength and is also in accordance with previous reports.[37,40]

TABLE III
Chain Relaxation Parameters Obtained from DMA Testing for IPC Samples

Sample	T_{EPR} (°C)	T_{iPP} (°C)	$T_{\alpha c}$ (°C)	I_R[a] (Rel. unit)
α-IPC	−32.9	23.9	96.6	0.345
β-IPC	−33.8	17.8	89.4	0.643

[a] I_R: peak area of glass transition of iPP.

From the results obtain by SEM and AFM, it can be concluded that smaller domain size (finer distribution) of the EPR-rich phase is achieved in β-IPC in comparison with the α-nucleated counterpart. It has been reported that for rubber particles with size of above 0.5 μm, the smaller the particle size, the lower the BDTT.[41,42] Thus, the phase morphology difference between α- and β-IPC samples may be one of the main reasons for their variants in impact resistance especially in BDTT. According to the theory proposed by Chen et al.,[43] the brittle-ductile transition is viewed as a competition between yielding and crazing with changes in the temperature and is dependent on activation of molecular motions of the matrix. Hence, the improvement in chain mobility in β-IPC, that is, the decrease of T_{iPP} and $T_{\alpha c}$, may be another reason for lowering of its BDTT.

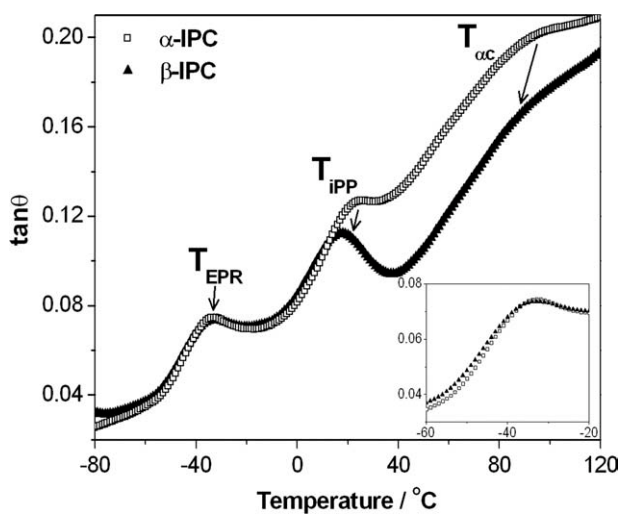

Figure 6 DMA loss factor profiles for the α- and β- IPCs; the inset shows enlarged area of T_{EPR}.

CONCLUSIONS

In summary, the IPCs with dominantly α- and β-modifications are prepared by introducing of small amounts of α- and β-nucleating agents, respectively. Their differences in BDTT as well as phase morphology are comparatively investigated. It is found that the BDTT is much lower for β-IPC than that for α-IPC. The subsequent morphological characterizations demonstrate a better dispersion of the EPR-rich phase in the β-IPC. From the aspect of competition between crystallization and LLPS, one of the possible reasons is thought to be the faster growth rate of β-spherulite that induces shorter segregation distance of the EPR-rich components, which leads to less aggregated EPR-rich phase in β-IPC. During crystallization process, the noncrystalline component is rejected into the interlamellar region of the crystalline phase, as well as being excluded into the interfibrillar and interspherulitic regions. The looser lamellar arrangement of the β-crystals is in favorite

of including more content of EPR-rich phase in the interlamellar regions, which is proposed to be the other reason for better dispersion of EPR-rich phase. Meanwhile, the inclusion of EPR-rich components in the interlamellar phase results in improved mobility of the amorphous PP chains as well as further increased impact strength for β-IPC and may also be one of the reasons for the shift of BDTT to lower temperature. Our works suggested a novel strategy to extend the lower limitation of service temperature without the sacrifice of rigidity at normal temperature, which may have important implications for designing and manufacturing high performance PP alloys.

References

1. Zuiderduin, W. C. J.; Westzaan, C.; Huéink, J.; Gaymans, R. J. Polymer 2003, 44, 261.
2. Tam, W. Y.; Cheung, T.; Li, R. K. Y. Polym Test 1996, 15, 363.
3. Galli, P.; Haylock, J. C. Prog Polym Sci 1991, 16, 443.
4. Urdampilleta, I.; González, A.; Iruin, J. J.; de la Cal, J. C.; Asua, J. M. Macromolecules 2005, 38, 2795.
5. Song, S. J.; Feng, J. C.; Wu, P. Y.; Yang, Y. L. Macromolecules 2009, 42, 7067.
6. Zhou, Y.; Niu, H.; Kong, L.; Zhao, Y.; Dong, J. Y.; Wang, D. J. Polymer 2009, 50, 4690.
7. Zhang, C. H.; Shangguan, Y. G.; Chen, R. F.; Wu, Y. Z.; Chen, F.; Zheng, Q. A.; Hu, G. H. Polymer 2010, 51, 4969.
8. Crevecoeur, G.; Groeninckx, G. Macromolecules 1991, 24, 1190.
9. Keith, H. D.; Padden, F. J. J Appl Phys 1964, 35, 1270.
10. Keith, H. D.; Padden, F. J. J Appl Phys 1964, 35, 1286.
11. Inaba, N.; Sato, K.; Suzuki, S.; Hashimoto, T. Macromolecules 1986, 19, 1690.
12. Inaba, N.; Yamada, T.; Suzuki, S.; Hashimoto, T. Macromolecules 1988, 21, 407.
13. Tanaka, H.; Nishi, T. Phys Rev Lett 1985, 55, 1102.
14. Tanaka, H.; Nishi, T. Phys Rev A 1989, 39, 783.
15. Niu, Y. H.; Wang, Z. G.; Orta, C. A.; Xu, D. H.; Wang, H.; Shimizu, K.; Hsiao, B. S.; Han, C. C. Polymer 2007, 48, 6668.
16. Zhang, X. H.; Man, X. K.; Han, C. C.; Yan, D. D. Polymer 2008, 49, 2368.
17. Ma, Y.; Zha, L.; Hu, W.; Reiter, G.; Han, C. C. Phys Rev E 2008, 77, 061801.
18. Padden, F. J.; Keith, H. D. J Appl Phys 1973, 44, 1217.
19. Lotz, B.; Wittmann, J. C. J Polym Sci Part B: Polym Phys 1986, 24, 1541.
20. Khoury, F. J Res Nat Bur Stand: A Phys Chem 1966, 70, 29.
21. Grigoryeva, O. P.; Karger-Kociss, J. Euro Polym J 2000, 36, 1419.
22. Chen, Y. H.; Mao, Y. M.; Li, Z. M.; Hsiao, B. S. Macromolecules 2010, 43, 6760.
23. Luo, F.; Geng, C. Z.; Wang, K.; Deng, H.; Chen, F.; Fu, Q.; Na, B. Macromolecules 2009, 42, 9325.
24. Varga, J. J Mater Sci 1992, 27, 2557.
25. Lotz, B. Polymer 1998, 39, 4561.
26. Chen, Y. H.; Zhong, G. J.; Wang, Y.; Li, Z. M.; Li, L. B. Macromolecules 2009, 42, 4343.
27. Bai, H. W.; Wang, Y.; Song, B.; Fan, X. M.; Zhou, Z. W.; Li, Y. L. Polym Bull 2009, 62, 405.
28. Bai, H. W.; Wang, Y.; Song, B.; Li, Y. L.; Liu, L. J Polym Sci Part B: Polym Phys 2008, 46, 577.
29. Grein, C.; Bernreitner, K.; Hauer, A.; Gahleitner, M.; Neißl, W. J Appl Polym Sci 2003, 87, 1702.
30. Grein, C.; Gahleitner, M. eXPRESS Polym Lett 2008, 2, 392.
31. Li, J. X.; Cheung, W. L.; Jia, D. Polymer 1999, 40, 1219.
32. Turner-Jones, A.; Aizelwood, J. M.; Beckett, D. R. Makromol Chem 1964, 75, 134.
33. Olley, R. H.; Bassett, D. C. Polymer 1982, 23, 1707.
34. Strobl, R. S.; Schneider, M. J.; Voigt-Martin, I. G. J Polym Sci Part B: Polym Phys 1980, 18, 1361.
35. Li, Y.; Xu, J. T.; Dong, Q.; Fu, Z. S.; Fan, Z. Q. Polymer 2009, 50, 5134.
36. Khambatta, F. B.; Warner, F.; Russell, T.; Stein, R. S. J Polym Sci Part B: Polym Phys 1976, 14, 1391.
37. Labour, T.; Gauthier, C.; SegueLa, R.; Vigier, G.; Bomal, Y.; Orange, G. Polymer 2001, 42, 7127.
38. Jafari, S. H.; Gupta, A. K. J Appl Polym Sci 2000, 78, 926.
39. Karger-Kocsis, J.; Kuleznev, V. N. Polymer 1982, 23, 699.
40. Grein, C. Adv Polym Sci 2005, 188, 43.
41. Corté, L.; Beaume, F.; Leibler, L. Polymer 2005, 46, 2748.
42. Bucknall, C. B.; Paul, D. R. Polymer 2009, 50, 5539.
43. Chen, L. P.; Yee, A. F.; Moskala, E. J. Macromolecules 1999, 32, 5944.